

Supporting Information

Perfluoroarene-Based 2D/3D Perovskite Solar Cells

Weifan Luo^{1#}, Jong-Min Kim^{2#}, Paul Zimmermann³, Tim Hügli¹, Sun-Ju Kim², Mengqiong Zhu¹, Ghewa AlSabeh^{1,4}, Alexander Hinderhofer³, Frank Schreiber³, Jovana V. Milić^{1}, Ji-Youn Seo^{2*}*

¹Adolphe Merkle Institute/ University of Fribourg, 1700 Fribourg, Switzerland; ²Department of Nanoenergy Engineering, Pusan National University, 46241 Busan, South Korea; ³Institute of Applied Physics, University of Tübingen, 72076 Tübingen, Germany; ⁴Laboratory of Photonics and Interfaces, École Polytechnique Fédérale de Lausanne, 1015 Lausanne, Switzerland. [#]These authors contributed equally. *Corresponding author: jovana.milic@unifr.ch, j-y.seo@pusan.ac.kr

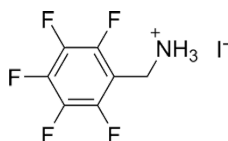
Table of Contents

Experimental Section	2
Supporting data	6
Reference	22

Experimental Section

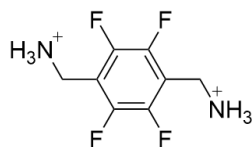
Materials

Cesium iodide (CsI) and hydrogen iodide (HI) aqueous solutions (57%) were purchased from Sigma Aldrich. Lead iodide (PbI₂) was purchased from Alfa Co. Ltd. Formamidineum iodide (FAI), methylammonium bromide (MABr) and 2,2',7,7'-tetrakis[*N,N*-di(4-methoxyphenyl)-amino]-9,9'-spirobifluorene (spiro-OMeTAD) were purchased from Lumtec. Ultra-dry *N,N*-dimethylformamide (DMF), ultra-dry dimethyl sulfoxide (DMSO), ethanol (EtOH), and ultra-dry chlorobenzene (CB) were purchased from Acros. Dry isopropanol (IPA), diethyl ether (DEE), 4-*tert*-butyl pyridine (tbp), lithium bistrifluorosulfonyl imide (Li-TFSI), acetylacetone, phenethylamine and titanium diisopropoxide bis(acetylacetonate), 75 weight % in IPA were purchased from Sigma-Aldrich. All the chemicals were used as received without further purification. Conductive glass, FTO (10 ohms/sq), was purchased from Nippon Sheet Glass, and titanium dioxide paste (30 NR-D) was purchased from Dyesol.



(*Perfluorophenyl*)methylaminium iodide (**F-BNAI**) was synthesised by following the previously reported procedure.¹ 2,3,4,5,6-pentafluorobenzonitrile (500 mg, 0.319 mL, 2.59 mmol) was added in a round bottom flask and flushed with nitrogen. BH₃ (1.0 M in THF, 6.5 mL, 6.5 mmol) was added dropwise to a suspension of 2,3,4,5,6-pentafluoro-benzonitrile in anhydrous THF (5 mL) at 0 °C. The mixture was stirred for 12 h before EtOH (10 mL) was added with vigorous stirring, and the solution was evaporated in vacuo. HI (0.85 mL, 6.47 mmol, 57%) was added at 0 °C, and a white precipitate formed immediately. After 6 h, EtOH (10 mL) was added, and the solution was concentrated in vacuo. DEE (150 mL) was then added to induce precipitation. The mixture was filtered, and the resultant solid was dried under vacuum to obtain **F-BNAI** as a white powder (460.8 mg, 54.75 %).

¹H NMR (400 MHz, (CD₃)₂SO): δ = 8.28 (bs, 3H), 4.18 (s, 2H) ppm; ¹³C NMR (101 MHz, (CD₃)₂SO): δ = 146.94–136.09, 108.5, 30.38 ppm; ¹⁹F NMR (377 MHz, (CD₃)₂SO): δ = -140.1, -152.5, -162.4 ppm



(*Perfluoro-1,4-phenylene*)dimethylammonium iodide (**F-PDMAI₂**) was synthesized following the previously reported procedure.²⁻³ 2,3,5,6-tetrafluoroterephthalonitrile (500 mg, 2.5 mmol) was added and flushed with nitrogen. BH₃ (1.0 M in THF, 11.24 mL, 11.24 mmol) was added dropwise to a suspension of 2,3,5,6-tetrafluoro-terephthalonitrile in anhydrous THF (15 mL) at 0 °C. The mixture was stirred for 36 h. After that, EtOH (20 mL) was added, and the solution was evaporated in vacuo to form a yellow solution. HI (1.48 mL, 11.24 mmol) was added at 0 °C and stirred for 6 h, resulting in a white suspension. The mixture was concentrated in vacuo to yield a white paste, over which EtOH (5 mL) was added, and the resultant suspension was added dropwise into DEE (150 mL). The mixture was allowed to crystallize overnight and it was filtered and washed with DEE (with a few drops of IPA added on the final wash). The resultant solid was dried under vacuum to obtain **F-PDMAI₂** (752 mg, 65%) as a white powder.

¹H NMR (400 MHz, (CD₃)₂SO): δ = 8.34 (bs, 6H), 4.24 (s, 4H) ppm; ¹³C NMR (101 MHz, (CD₃)₂SO): δ = 146.3–143.7, 114.5, 30.9 ppm; ¹⁹F NMR (377 MHz, (CD₃)₂SO): δ = -140.6 ppm

Perovskite thin film preparation

All samples were prepared in a glovebox under dry nitrogen atmosphere (0 ppm H₂O, 0.1–5 ppm O₂). Films were prepared on microscope glass or conductive fluorine doped tin oxide (FTO) glass, as indicated in the corresponding methods. The glass was cut from microscope slides to dimensions of 15x25 mm. The glasses were cleaned using Hellmanex (2%, deionized water), deionized water, isopropanol (IPA), and ethanol by sonicating for 10–15 min. Subsequently, the substrates were dried with nitrogen and stored until use in a dry box. The substrates were cleaned in UV-ozone plasma for 5–10 min before solution deposition. Solutions of 1 mg/mL F-BNA-I in IPA, 1 mg/mL of F-PDMAI₂ in IPA, and 0.4 M (F-BNA)₂PbI₄ or 0.4 M (F-PDMA)PbI₄ in 4:1 DMF/DMSO, were prepared using stoichiometric amounts of the precursors followed by heating to 60 °C. 40 µl of the respective solution was spread on the glass before starting the spin-coating program with a maximum rotation speed of 4000 rpm and acceleration of 2000 rpm/s with a duration of 20 s, followed by annealing at 130 °C for 10 min.

Device preparation

Etched fluorine-doped tin oxide (FTO) conductive glasses were used for device preparation. They were cleaned using Hellmanex (2%, deionized water), deionized water, isopropanol, and ethanol by sonicating for 10–15 min for each solvent. Subsequently, the glasses were dried with a nitrogen gun and stored until use in a dry box. Before further processing, the glass substrates were cleaned in UV-ozone plasma for 5–10 min.

As part of an electron-conducting layer, a compact TiO_2 (c- TiO_2) layer was deposited on the glasses using spray pyrolysis with O_2 as a carrier gas. The substrates were preheated to 450 °C, and a precursor solution consisting of 0.6 mL titaniumdiisopropoxide bis(acetylacetonate), 75 wt% in IPA, 0.4 mL acetylacetone and 9 mL dry ethanol was used. After the spray pyrolysis, the TiO_2 coated glasses were kept at 450 °C for 5 min before cooling down to room temperature. On top of the compact TiO_2 layer, a mesoporous TiO_2 (m- TiO_2) layer was deposited by spin coating for 20 s at 4000 rpm with an acceleration of 2000 rpm/s. For the m- TiO_2 layer, a solution of TiO_2 paste (30NRD, Dyesol) diluted in anhydrous ethanol at a weight ratio of 1:6 was used. After drying at 100 °C, the glasses were sintered at 450 °C for 30 min.

The perovskite precursor solution was prepared by dissolving a mixture of PbI_2 (1.61 mmol, 742.0 mg), FAI (1.31 mmol, 224.4 mg), MABr (0.15 mmol, 16.2 mg), and CsI (0.08 mmol, 19.8 mg) to yield $\text{Cs}_{0.05}\text{FA}_{0.85}\text{MA}_{0.10}\text{Pb}(\text{I}_{0.97}\text{Br}_{0.03})_3$ with 5% excess of PbI_2 in 1 mL of a mixed solution of DMF and DMSO [DMF (v): DMSO (v) = 4:1] under mild heating conditions at 70 °C to assist dissolving. For precursor solutions containing MACl, 10 mol% was added. The perovskite precursor solution was deposited on the substrates via spin-coating using an antisolvent method with CB as the antisolvent. The spin-coating program consisting of two steps was carried out first with 2000 rpm and an acceleration rate of 200 rpm/s for 10 sec followed by 6000 rpm and an acceleration rate of 2000 rpm/s for 30 sec. CB (200 μL) was dripped 15 sec before the second step ended with a 1–2 sec depositing time. The samples were annealed at 120 °C for 20 min.

For F-BNAI and F-PDMAI₂ 2D/3D overlayer, 1 mg/mL of F-BNAI or F-PDMAI₂ were dissolved in IPA and 40 μL dynamically spin-coated on the surface of the perovskite layer at 4000 rpm for 20 s with 5 min annealing at 130 °C. *For samples treated with a MACl overlayer*, 4 mg/mL of MACl in IPA were dynamically coated at 4000 rpm for 20 s with 5 min annealing at 120 °C. The preparation was carried out in a dry air-filled glove box with a relative humidity of about 2%.

For the hole-transporting layer, Spiro-OMeTAD was dissolved in CB for a concentration of 77.6 mM. 1 mL spiro-OMeTAD solution was doped with 20.6 μL Li-TFSI (520 mg/mL in acetonitrile) and 35.5 μL tBP. The mixed spiro-OMeTAD solution was dynamically spin-coated on the surface of the perovskite at 4000 rpm for 20 sec.

The gold electrode was thermally evaporated under vacuum onto the spiro-OMeTAD layer of the samples with a shadow mask with an aperture area of 5 mm by 5 mm. The thickness of the gold electrode was adjusted to 80 nm.

Characterization

Grazing Incidence Wide Angle X-ray Scattering (GIWAXS) was measured at the ESRF synchrotron at Beamline BM01. For the scan a PILATUS2M detector was used and a Beam energy of 11.941 keV. The incident angle was scanned from 0-2° to obtain both surface and bulk sensitive data.

X-ray diffraction measurements were conducted using a PANalytical Empyrean Series 2 instrument in Bragg-Brentano configuration. The instrument utilized Cu K α radiation with a voltage of 40 kV and a current of 40 mA. For the specific purpose of grazing incidence measurements, the X-ray incidence angle was set at 2°. Diffracted X-rays were detected during the experiments employing a PIXcel3D detector.

X-ray photoelectron spectroscopy (AXIS SUPRA) was performed with an Al K α radiation source, and all binding energies were calibrated by C 1s (248.8 eV) as a reference.

UV-vis absorption spectroscopy was conducted using a Shimadzu UV-2600 spectrophotometer.

Photoluminescence spectroscopy was performed using a Fluorolog 322 spectrometer (Horiba Jobin Yvon iHr320) equipped with a CCD detector, using a slit width of 5 nm, and the excitation by a Xenon lamp at a wavelength of 350 nm. The band slit width during the measurements was set to 5 nm.

Time-Resolved Photoluminescence (TRPL) was measured via time-correlated single photon counting (TCSPC) using a LifeSpec II (Edinburgh Instruments) fluorescence spectrometer with a picosecond pulsed diode laser (EPL-510, Edinburgh Instruments) at 510 nm wavelength.

Supporting data

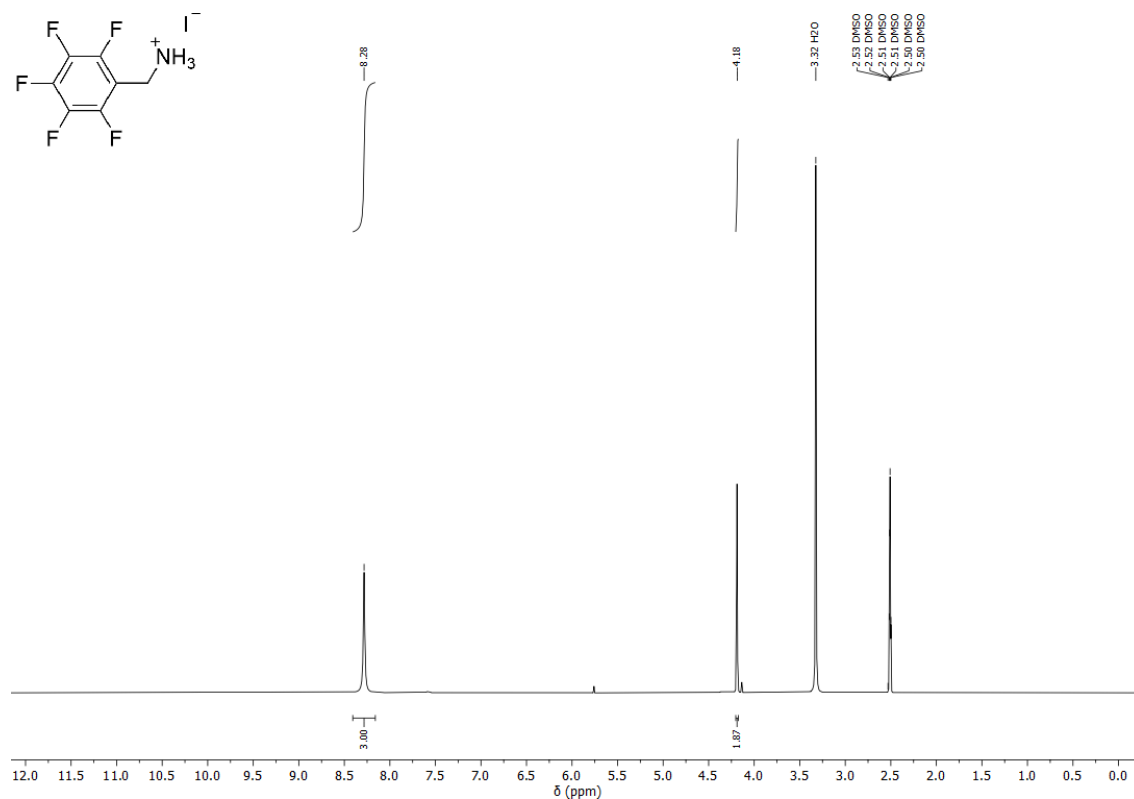


Figure S1. ¹H NMR of F-BNAI in (CD₃)₂SO (400 MHz, 298 K).

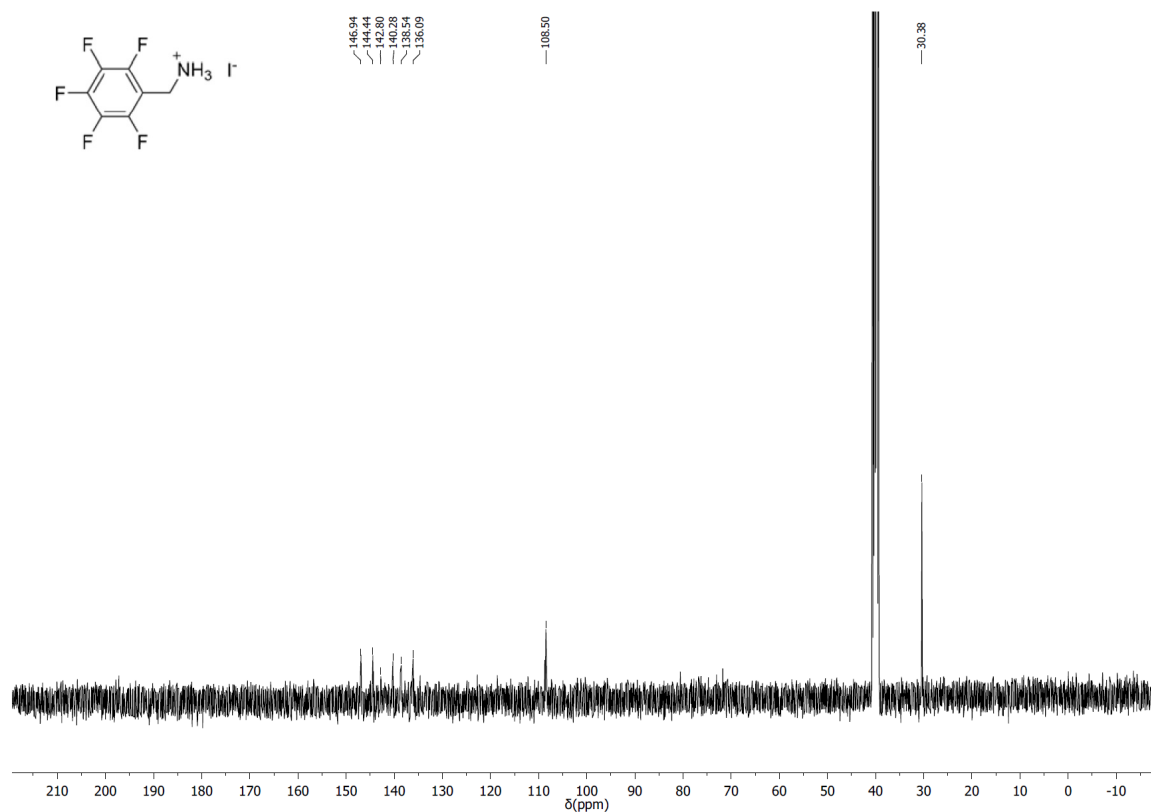


Figure S2. ¹³C NMR of F-BNAI in (CD₃)₂SO (101 MHz, 298 K).

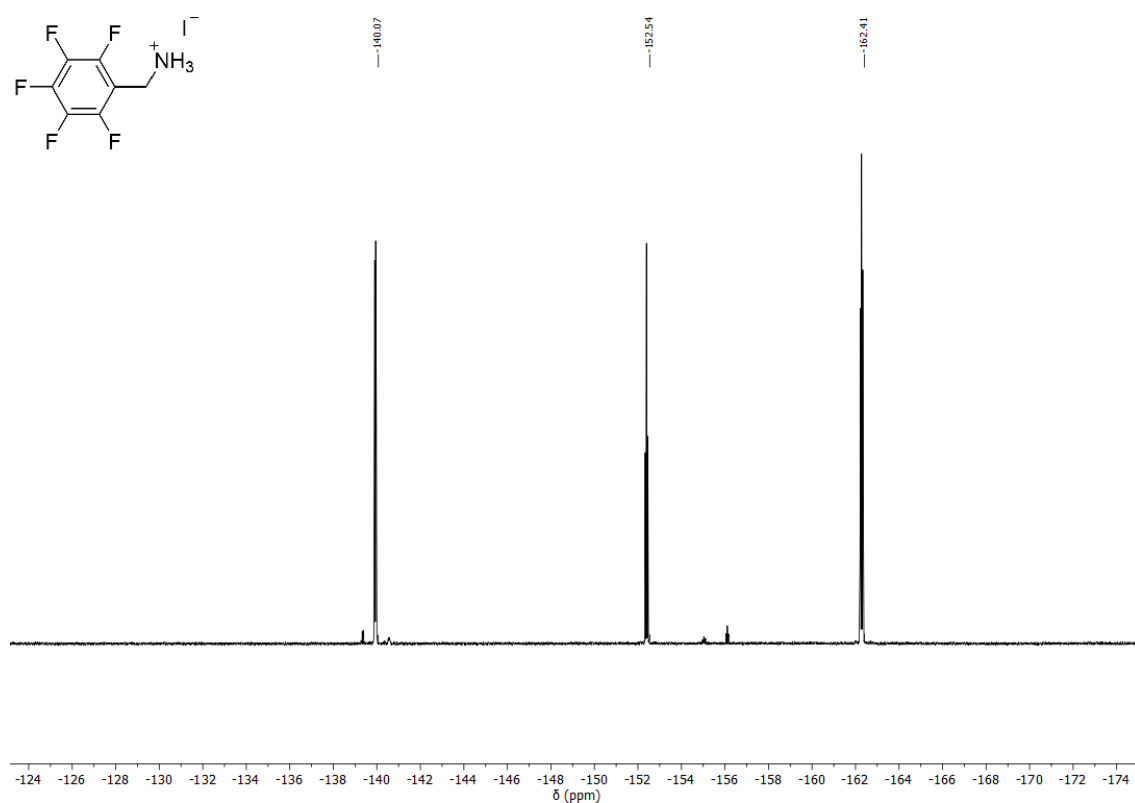


Figure S3. ^{19}F NMR of F-BNAI in $(\text{CD}_3)_2\text{SO}$ (377 MHz, 298 K).

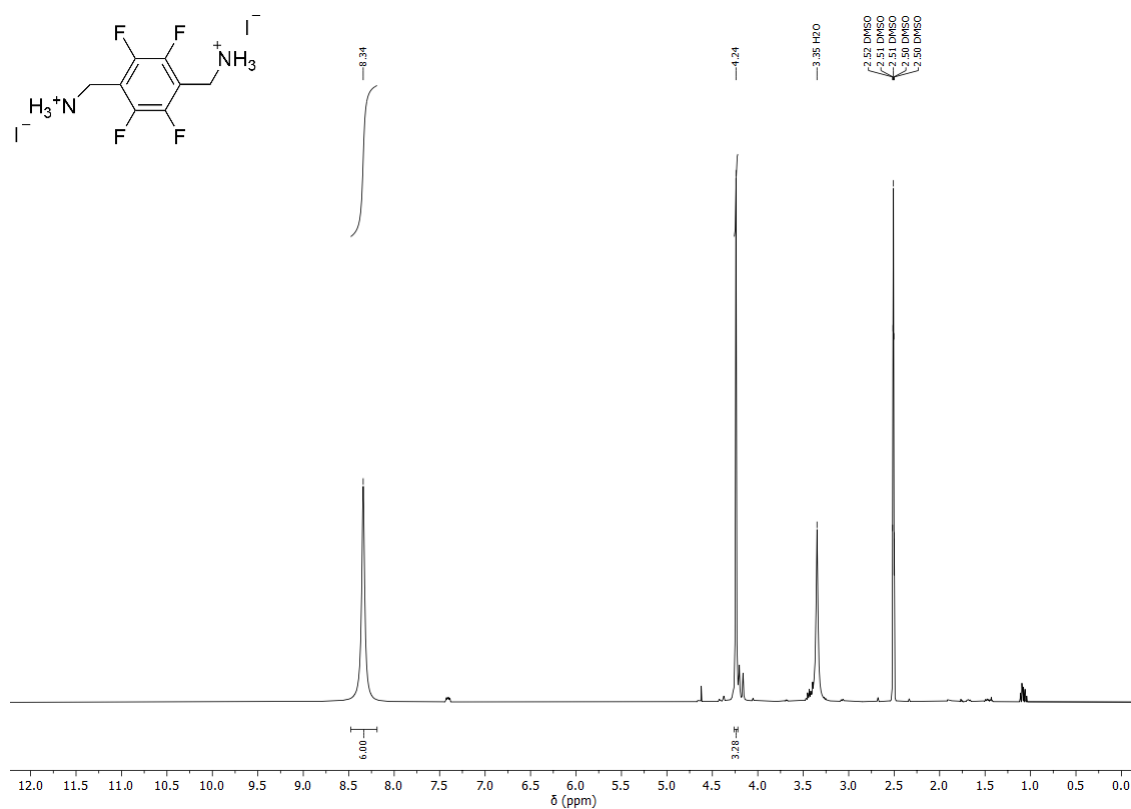


Figure S4. ^1H NMR of F-PDMAI in $(\text{CD}_3)_2\text{SO}$ (400 MHz, 298 K).

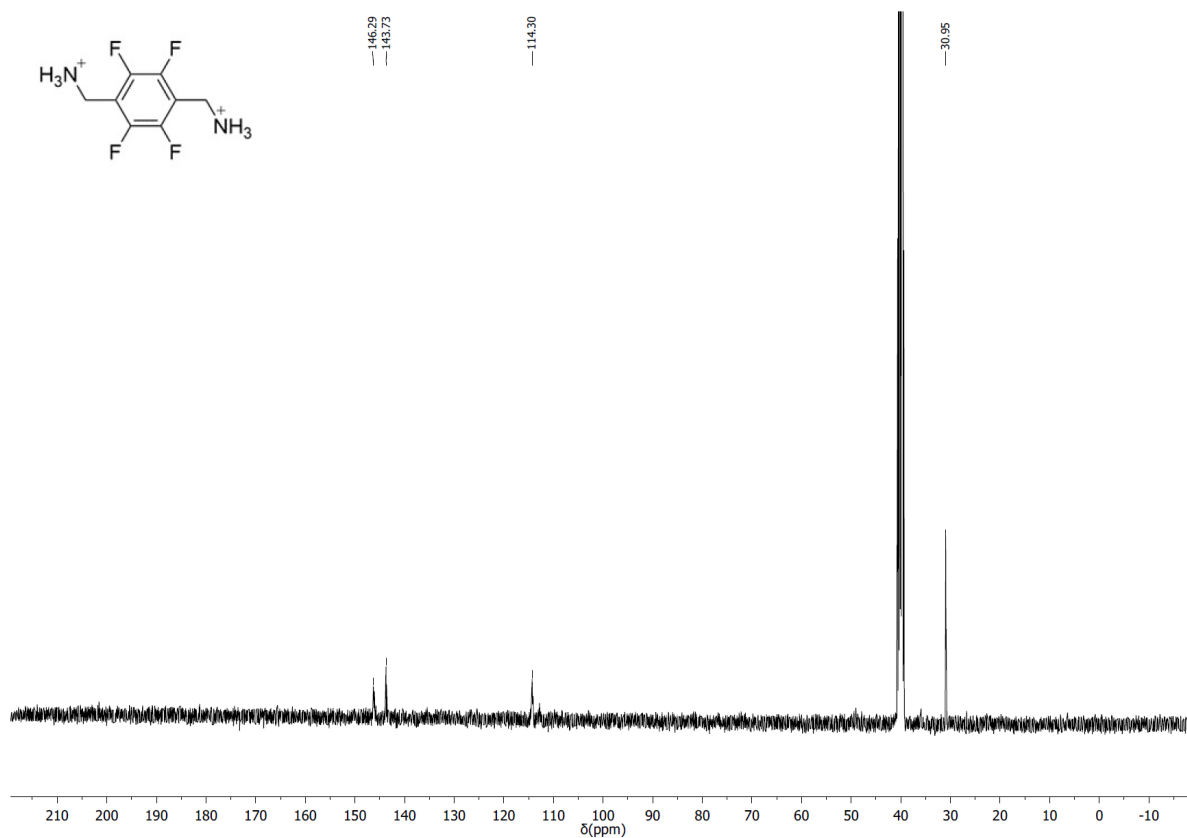


Figure S5. ¹³C NMR of F-PDMAI₂ in (CD₃)₂SO (101 MHz, 298 K).

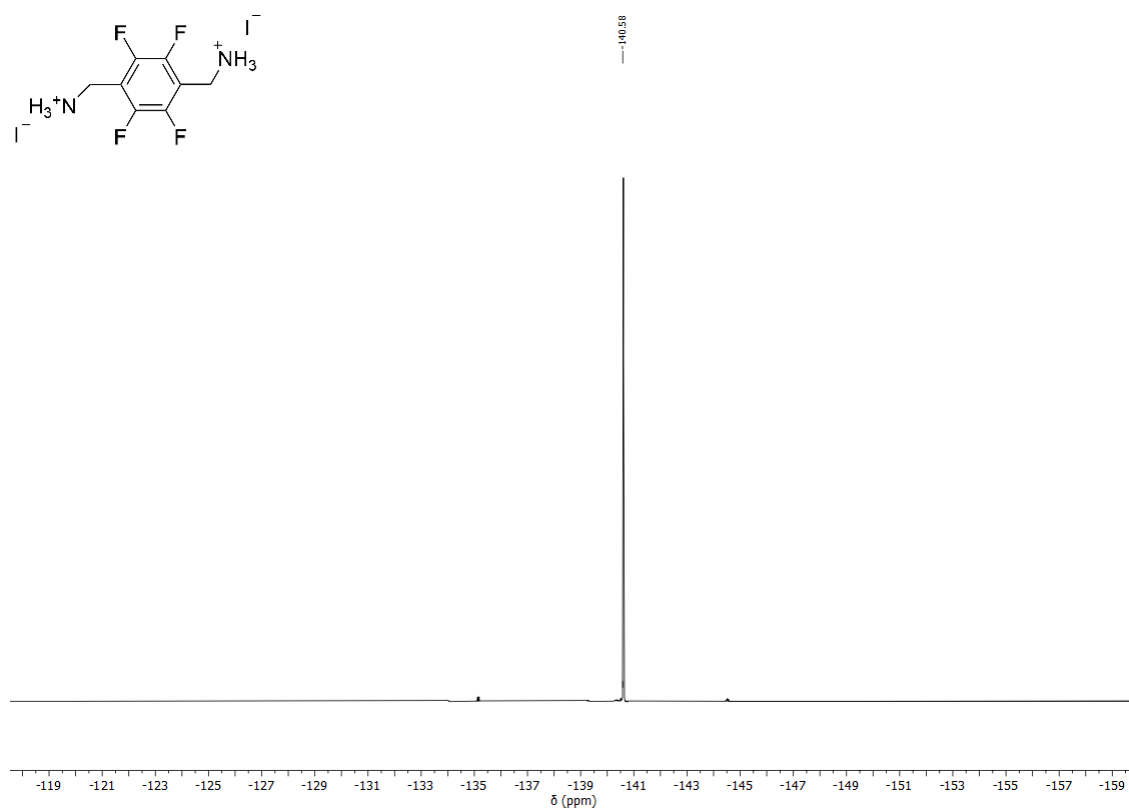


Figure S6. ¹⁹F NMR of F-PDMAI₂ in (CD₃)₂SO (377 MHz, 298 K).

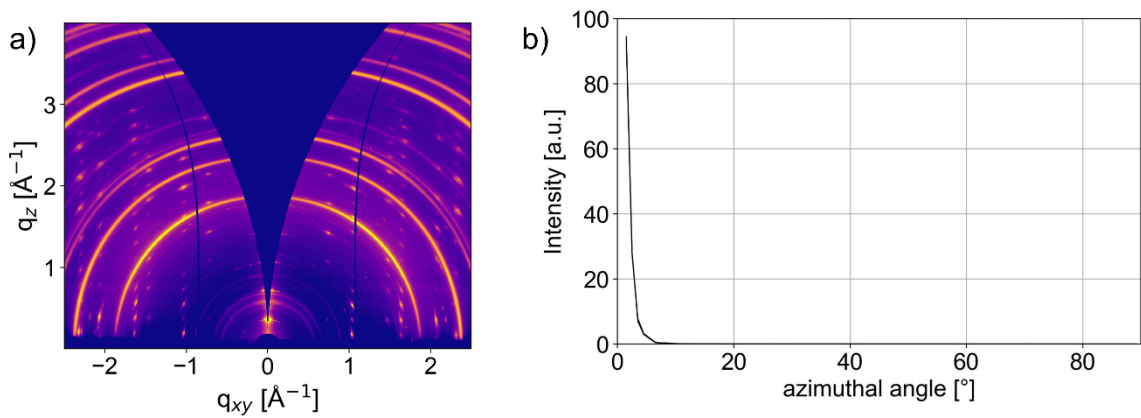


Figure S7. (a) GIWAXS reciprocal space maps of (F-BNA)₂PbI₄ film on glass and (b) the azimuthal profile of its first XRD peak at 0.35 Å⁻¹.

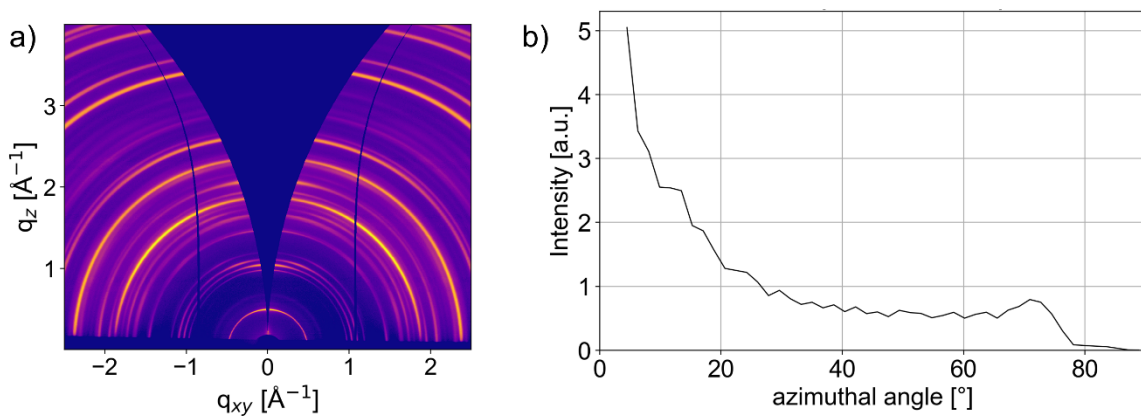


Figure S8. (a) GIWAXS reciprocal space maps of (F-PDMA)PbI₄ film on glass and (b) the azimuthal profile of its first XRD peak at 0.49 Å⁻¹.

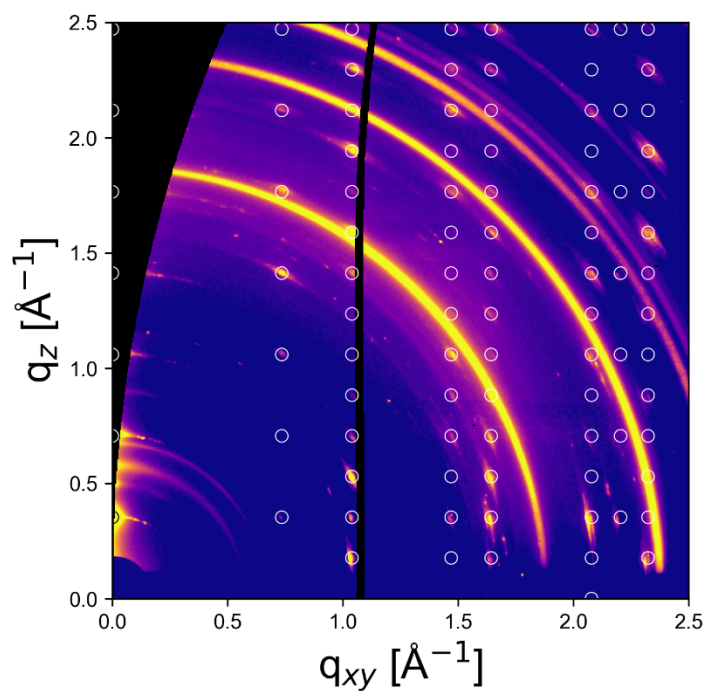


Figure S9. GIWAXS reciprocal space maps of (F-BNA)₂PbI₄ film on FTO covered glass. Circles correspond to the unit in Table S1 and coincide well with peaks from the 2D structure. Intense rings in the data originate from the FTO substrate.

Table S1. Unit cell parameters for (FBNA)₂PbI₄ (Error bars are estimated). Due to the fluorination of the spacer molecule, the unit cell is significantly larger than the unit cell of (BNA)₂PbI₄.⁴

Crystal Data	(FBNA) ₂ PbI ₄	(BNA) ₂ PbI ₄
a (Å)	8.55(8)	9.1561(5)
b (Å)	8.55(8)	8.6894(3)
c (Å)	35.6(4)	28.7762(15)
α (°)	90.0(5)	90
β (°)	90.0(5)	90.000(4)
γ (°)	90.0(5)	90
V (Å ³)	2602(78)	2289.46(19)

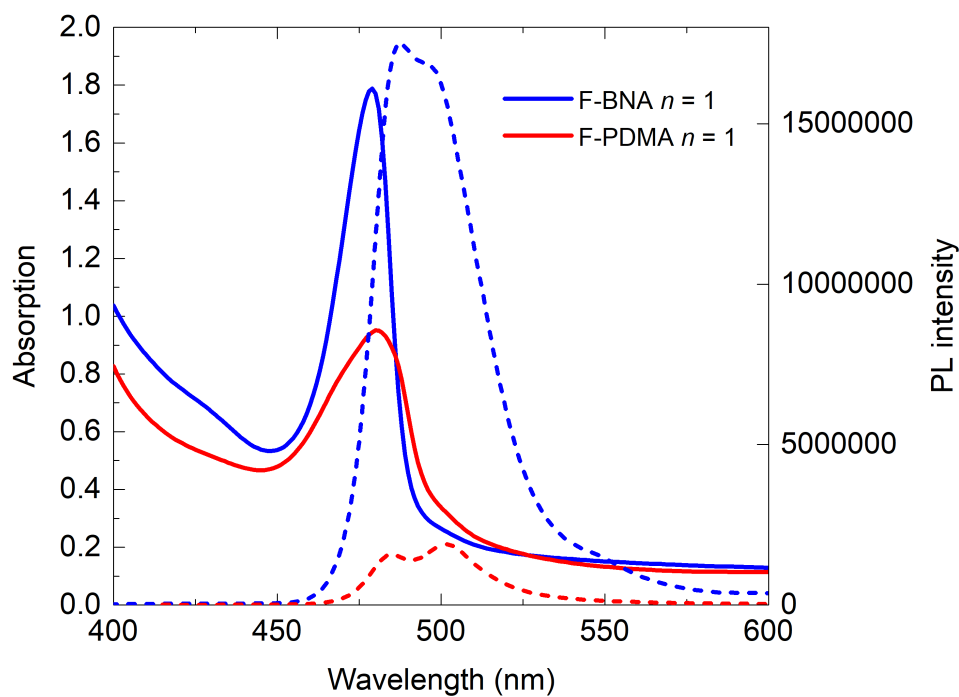


Figure S10. UV-vis absorption and PL raw spectra of the perfluoroarene-based 2D perovskite films of $n = 1$ nominal composition.

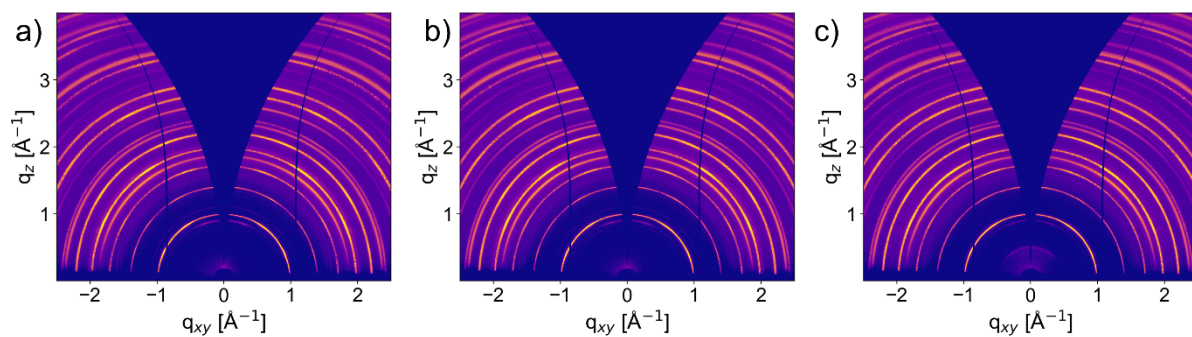


Figure S11. GIWAXS reciprocal space maps of (a) Control 3D, (b) (F-BNA)- and (c) (F-PDMA)- treated films on glass.

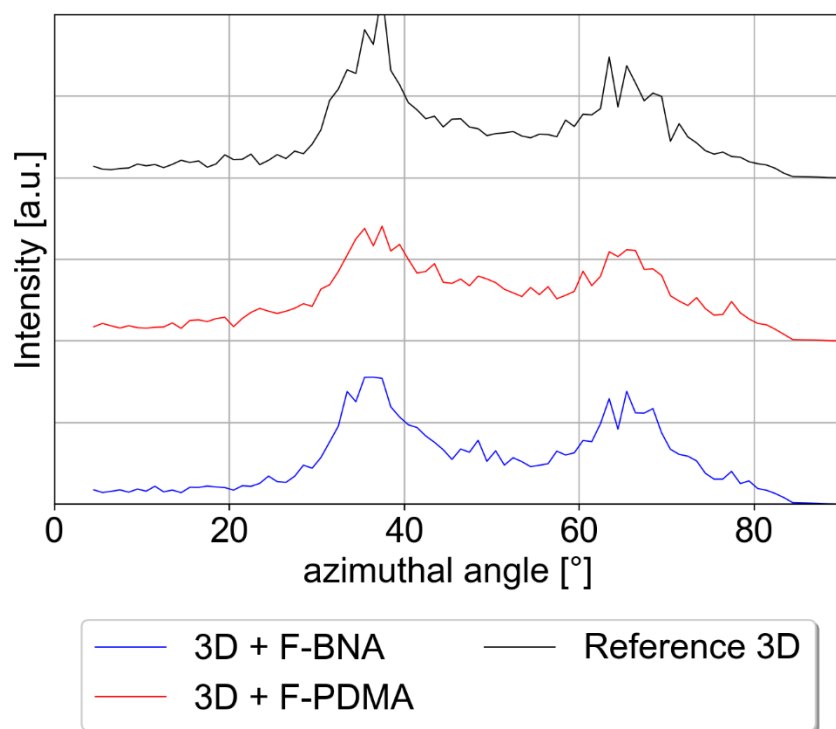


Figure S12 Azimuthal intensity profiles of the (001) perovskite peak from Figure S11.

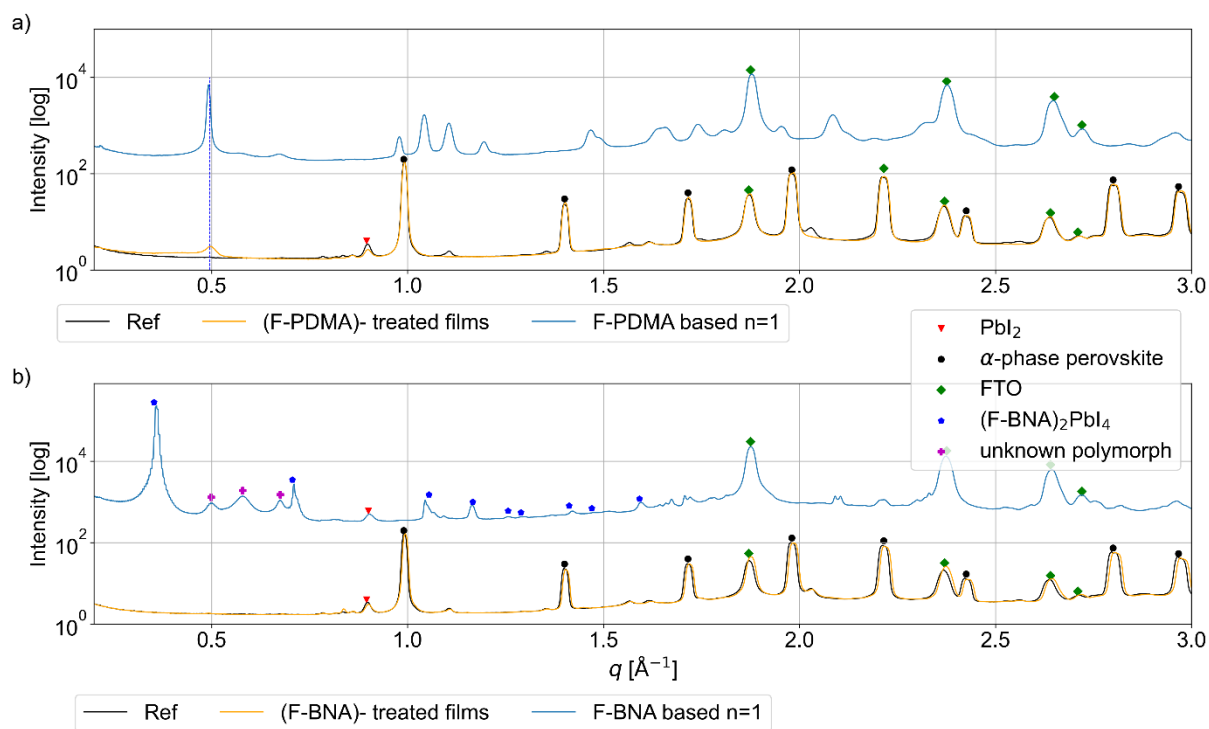


Figure S13. Radially integrated GIWAXS data of the a) (F-PDMA)PbI₄, Control and (F-PDMA)- treated film and b) (F-BNA)PbI₄, Control and (F-BNA)- treated film. Peaks marked with purple squares presumably originate from an (F-BNA)PbI₄ polymorph with low volume fraction.

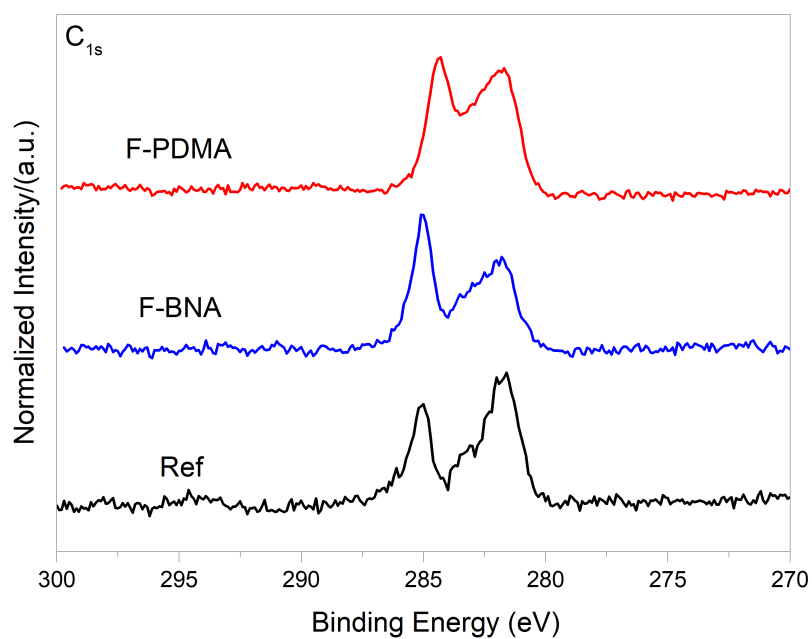


Figure S14. XPS C 1s core level spectra of the 3D perovskite films (Ref) and 3D/2D films with either F-PDMAI₂ (red) or F-BNAI (blue) overlayer on FTO glass.

Table S2. Full width at half maximum (FWHM) for XPS N 1s core level spectra (Figure 2d).

	FWHM (°)
F-PDMA	1.18
F-BNA	1.04
Reference	0.988

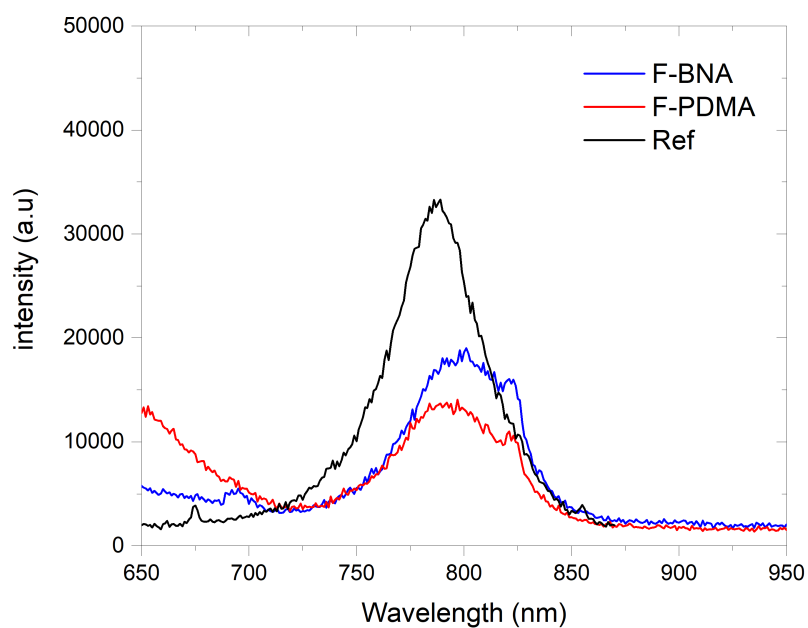


Figure S15. PL spectra of the 3D perovskite films (Ref) and 3D/2D films with either F-PDMAI₂ (red) or F-BNAI (blue) overlayer on microscope glass.

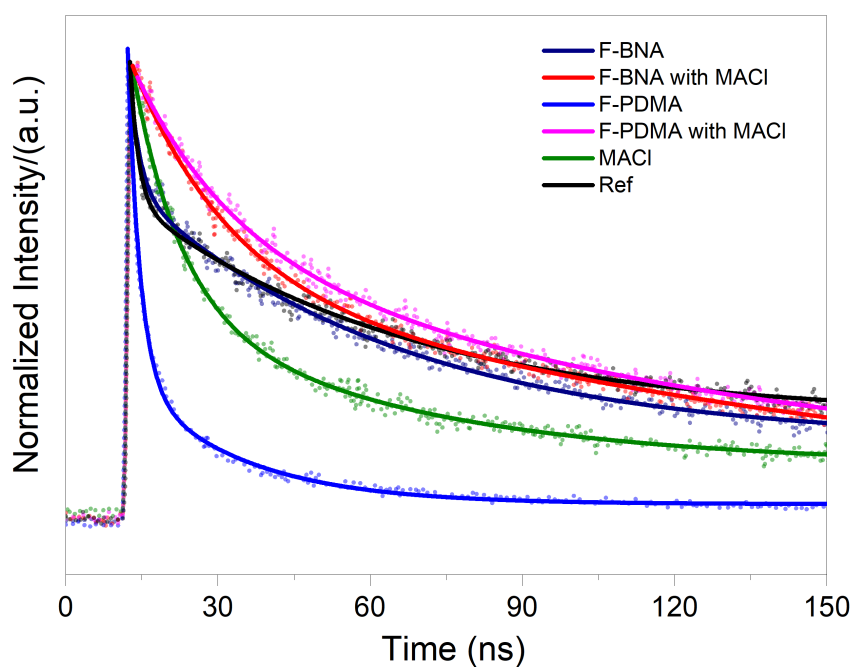


Figure S16. TRPL spectra of the 3D perovskite films (reference) and the 3D perovskite films treated with MACI additive and 3D/2D films with F-PDMAI₂ or F-BNAI overlayers on glass.

Table S3. Summary of the parameters from fitting to the TRPL decay data (without HTM)

	τ_1 (ns)	τ_2 (ns)
Ref	1.6	53.8
F-BNA	2	52.96
F-PDMA	21.81	2.44
Ref With MACl	9.49	51.14
F-BNA With MACl	0.58	19.65
F-PDMA With MACl	144.84	19.03

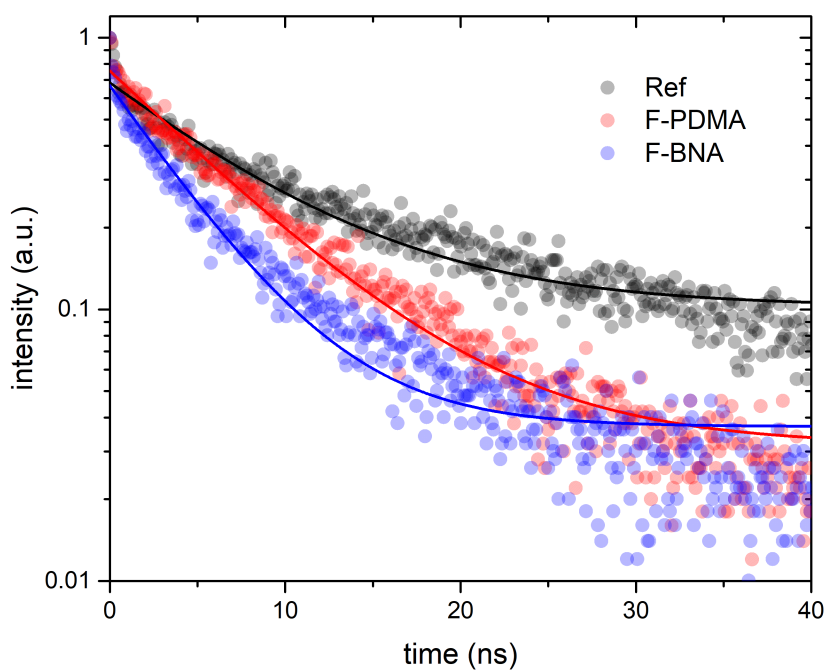


Figure S17. TRPL spectra of the 3D perovskite films (Ref) and 3D/2D films with either F-PDMAI₂ (red) or F-BNAI (blue) overlayer on microscope glass with HTM on top.

Table S4. Summary of the parameters from the fit of the TRPL decay (with HTM).

	τ_1 (ns)
Ref	7.9
F-BNA	4.6
F-PDMA	6.8

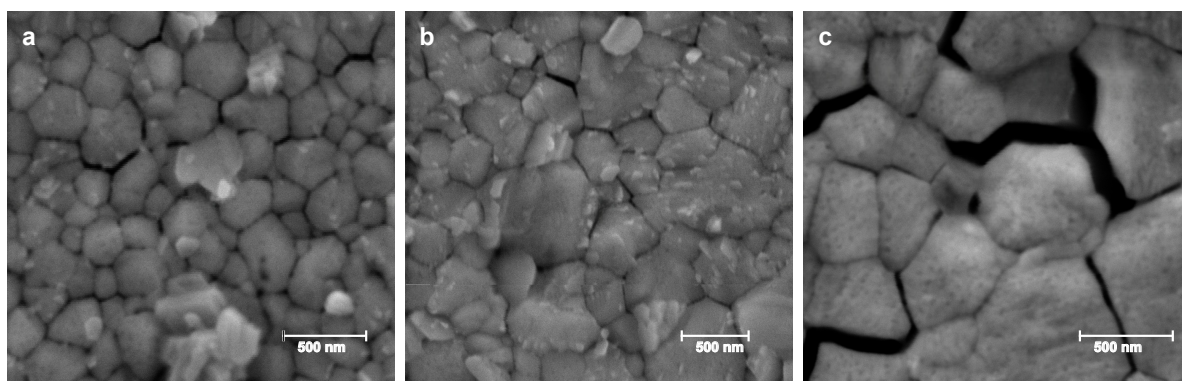


Figure S18. SEM image of the perovskite surface based on (a) 3D films (Ref) and (b–c) 2D/3D films treated with either F-BNAI (b) and (c) F-PDMAI₂ no FTO glass.

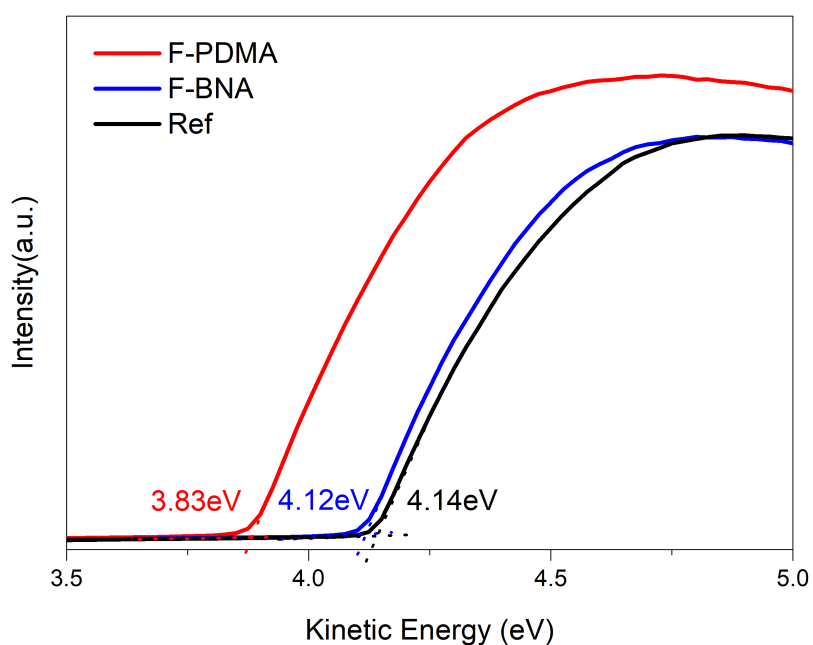


Figure S19. UPS spectra determining the kinetic energy around the secondary electron cut-off of the control (Ref) and treated (F-BNA or F-PDMA) perovskite films on FTO glass.

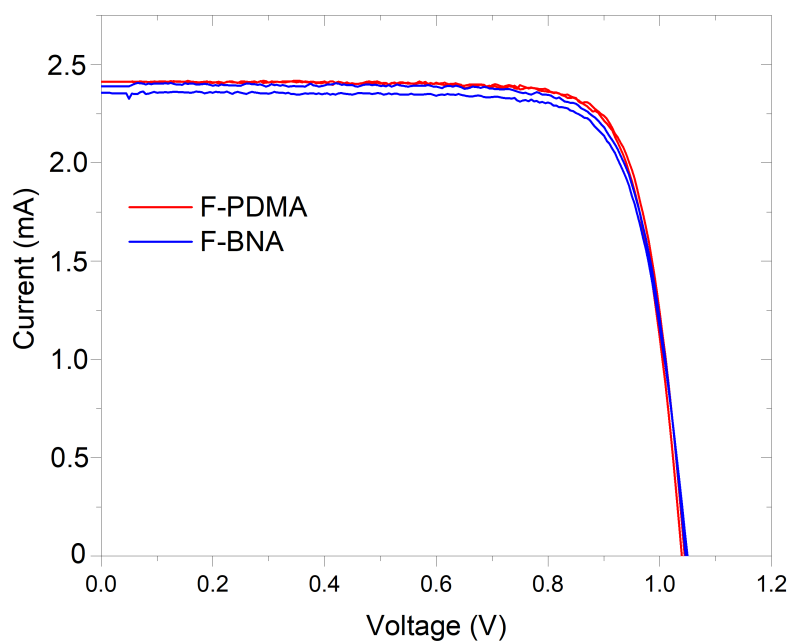


Figure S20. Current-voltage characteristics of the champion perovskite solar cells based on $(\text{Cs}_{0.05}\text{FA}_{0.85}\text{MA}_{0.10})\text{Pb}(\text{I}_{0.97}\text{Br}_{0.03})_3$ with an overlayer of F-BNAI or F-PDMAI₂.

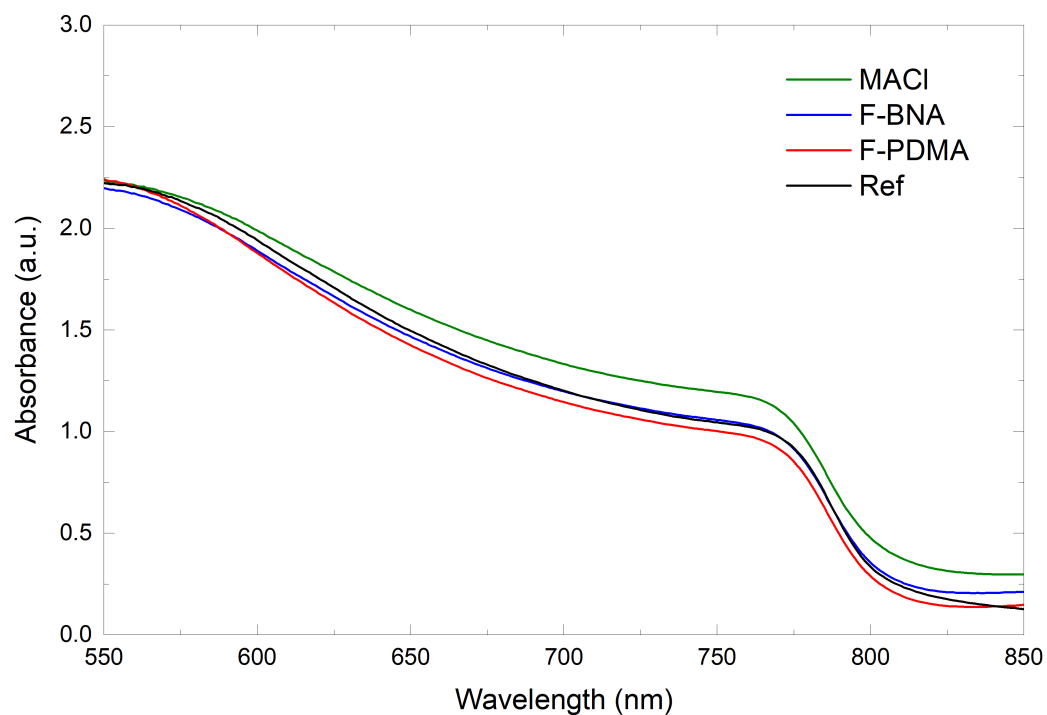


Figure S21. UV-vis spectra of the 3D perovskite films (Ref) and 3D/2D films with either F-PDMAI₂ (red) or F-BNAI (blue) overlayer in the presence of MACl additive on glass.

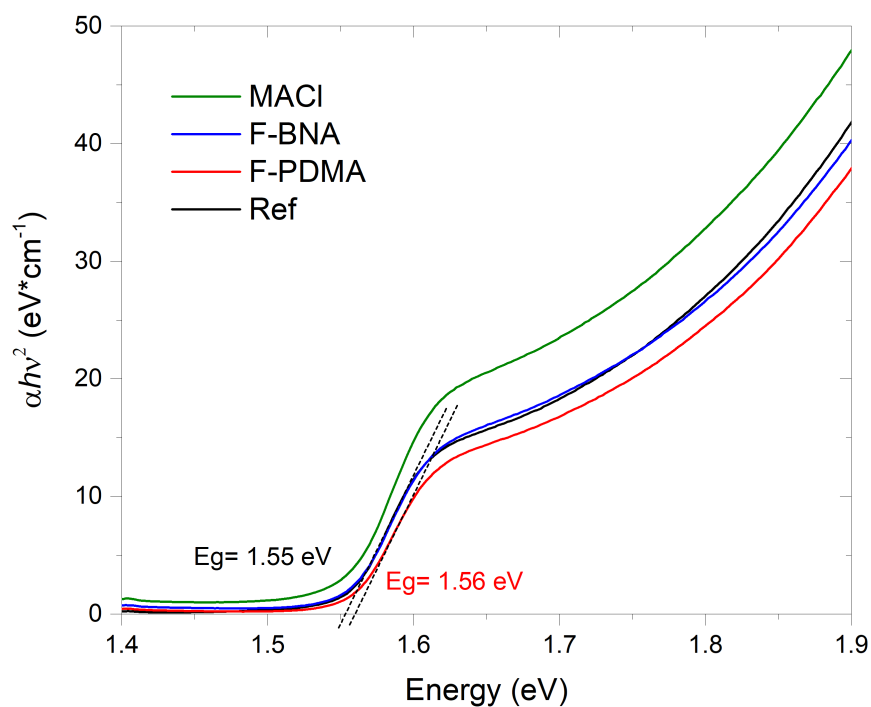


Figure S22. Tauc plot determining the optical band gap (E_g) for the 3D perovskite films (Ref) and 3D/2D films with either F-PDMAI₂ (red) or F-BNAI (blue) overlayer in the presence of MACI additive on glass.

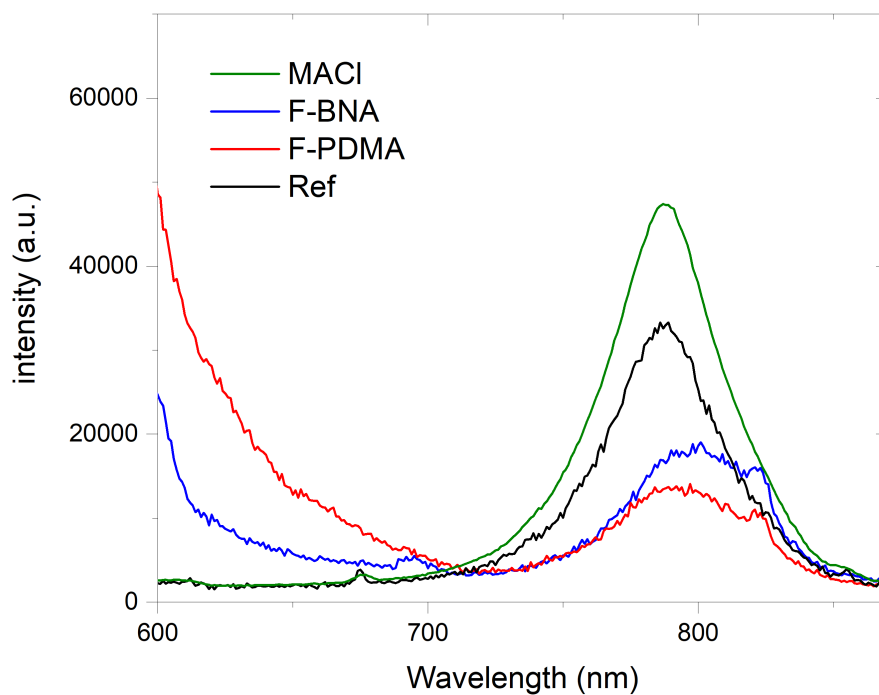


Figure S23. PL spectra of the 3D perovskite films (Ref) and 3D/2D films with either F-PDMAI₂ (red) or F-BNAI (blue) overlayer in the presence of MACI additive on microscope glass.

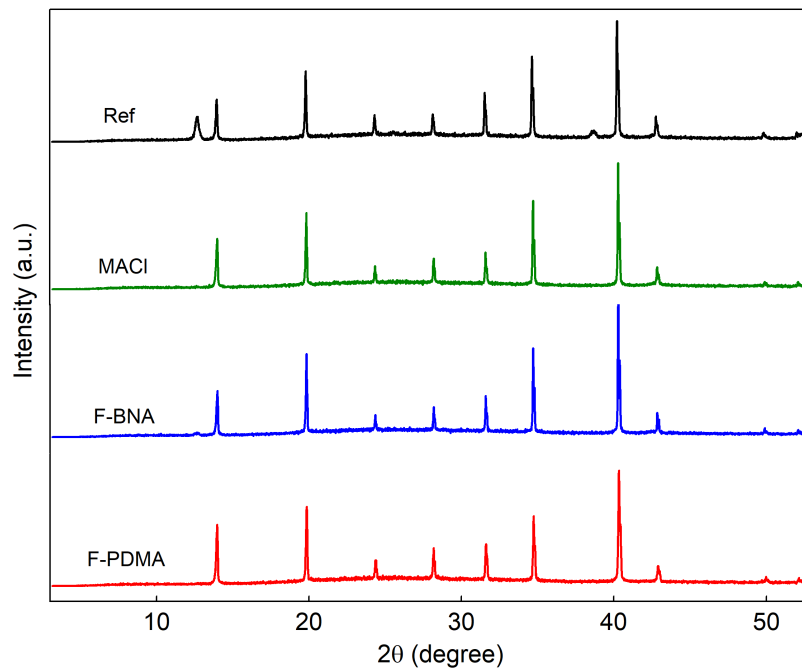


Figure S24. XRD pattern of the 3D perovskite films (Ref) and 3D/2D films with either F-PDMAI₂ (red) or F-BNAI (blue) overlayer in presence of MACl additive on microscope glass.

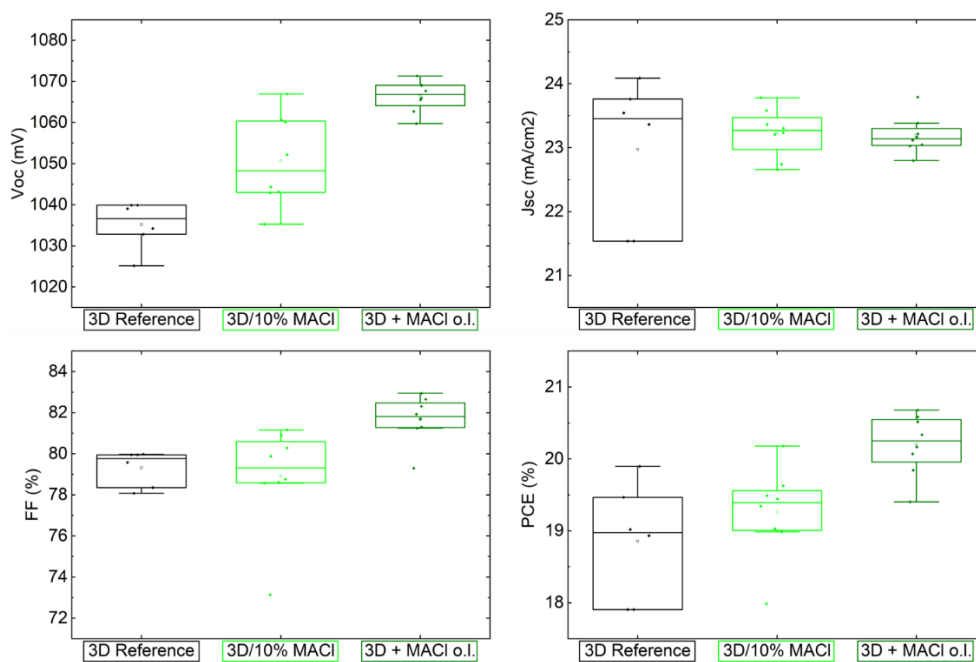


Figure. S25. Statistical distribution of photovoltaic metric, including open-circuit voltage (V_{oc}), short-circuit current density (J_{sc}), fill factor (FF), and power conversion efficiency (PCE) for control (3D Reference) and MACl-treated devices as an additive (10%) and an overlayer (o.l.).

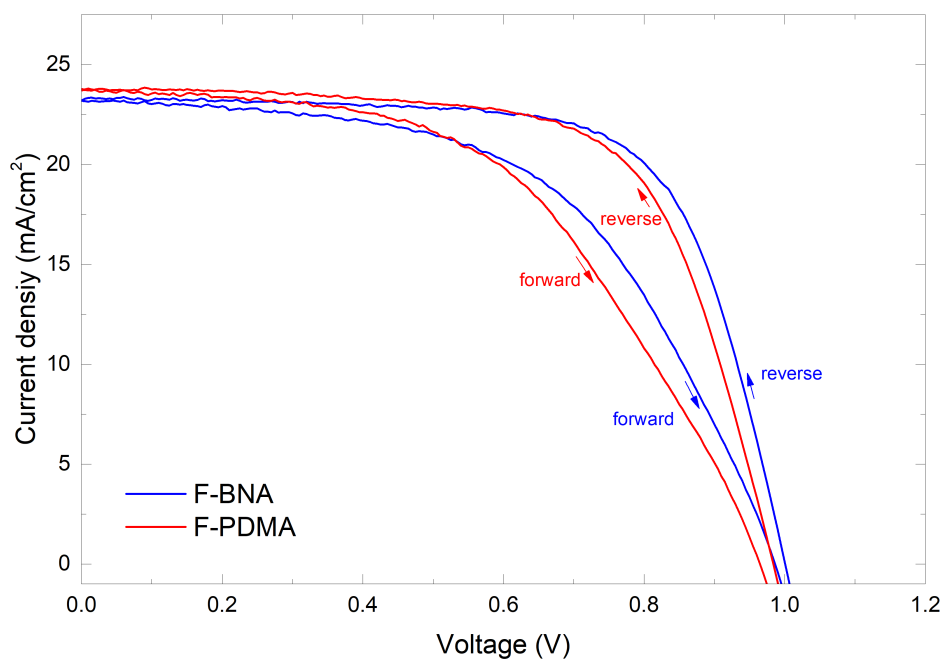


Figure S26. Current-voltage characteristics of the champion perovskite solar cells based on $\text{Cs}_{0.05}\text{FA}_{0.85}\text{MA}_{0.10}\text{Pb}(\text{I}_{0.97}\text{Br}_{0.03})_3$ with MACl additive treated with F-BNAI or F-PDMAI₂.

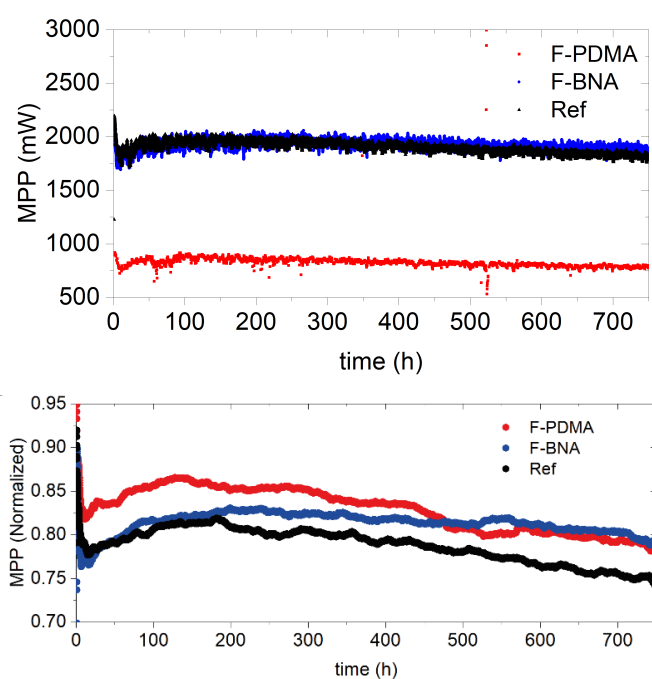


Figure S27. Evolution of the PCE during operation by MPP tracking (top) and normalized performance (bottom) of control (black), F-BNA (blue) and F-PDMA (red) treated perovskite solar cells in N_2 atmosphere under 1 sun irradiation at ambient temperature.

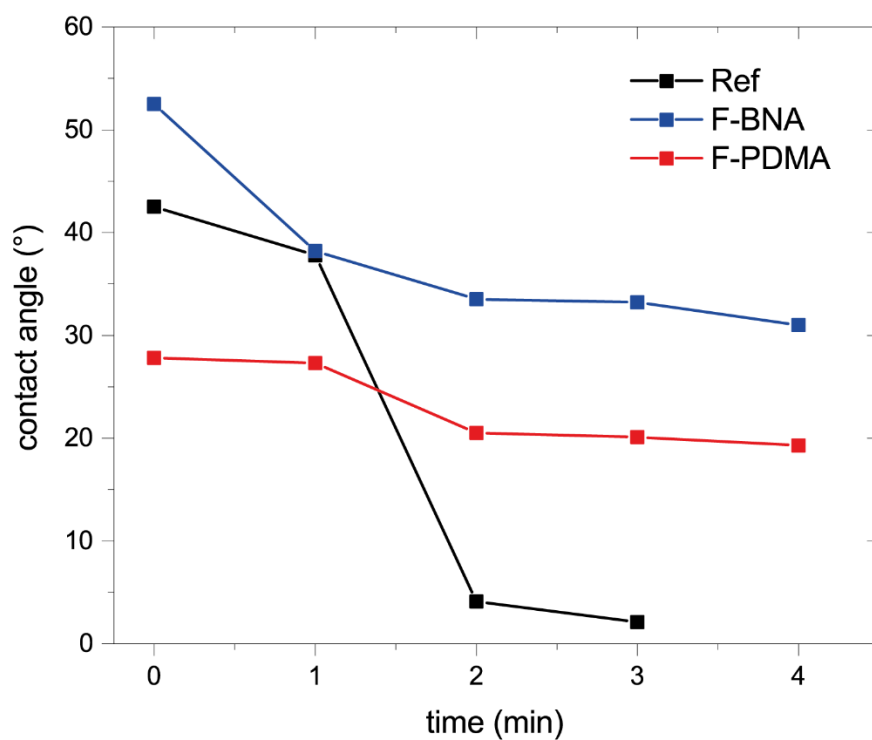
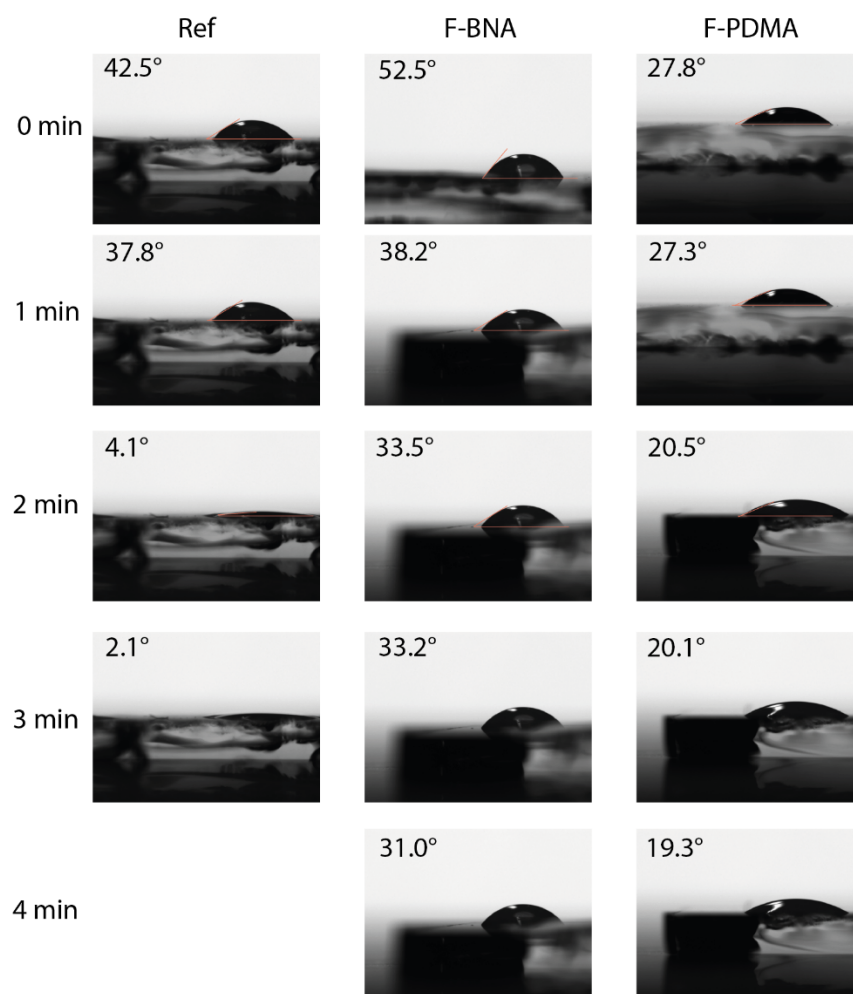


Figure S28. Contact angle measurement of a water drop on the surface of 3D perovskite films (Ref) and 3D/2D films with either F-PDMAI₂ (red) or F-BNAI (blue) overlayer on glass.

Table S5. Summary of the photovoltaic parameters of the champion devices.

Device	V _{oc} (V)	J _{sc} (μA)	FF	PCE
Control	1.05	2183	80.0%	18.4%
F-BNA	1.06	2389	80.1%	20.0%
F-PDMA	1.05	2413	79.9%	20.0%

Reference

- (1) Almalki, M.; Dučinskas, A.; Carbone, L. C.; Pfeifer, L.; Piveteau, L.; Luo, W.; Lim, E.; Gaina, P. A.; Schouwink, P. A.; Zakeeruddin, S. M. Nanosegregation in arene-perfluoroarene π -systems for hybrid layered Dion–Jacobson perovskites. *Nanoscale* **2022**, *14*, 6771–6776.
- (2) Hope, M. A.; Nakamura, T.; Ahlawat, P.; Mishra, A.; Cordova, M.; Jahanbakhshi, F.; Mladenović, M.; Runjhun, R.; Merten, L.; Hinderhofer, A.; Carlsen, B. I.; Kubicki, D. J.; Gershoni-Poranne, R.; Schneeberger, T.; Carbone, L. C.; Liu, Y.; Zakeeruddin, S. M.; Lewinski, J.; Hagfeldt, A.; Schreiber, F.; Rothlisberger, U.; Grätzel, M.; Milić, J. V.; Emsley, L. Nanoscale Phase Segregation in Supramolecular π -Templating for Hybrid Perovskite Photovoltaics from NMR Crystallography. *J. Am. Chem. Soc.* **2021**, *143*, 1529–1538.
- (3) Li, Y.; Milić, J. V.; Ummadisingu, A.; Seo, J.-Y.; Im, J.-H.; Kim, H.-S.; Liu, Y.; Dar, M. I.; Zakeeruddin, S. M.; Wang, P.; Hagfeldt, A.; Grätzel, M. Bifunctional Organic Spacers for Formamidinium-Based Hybrid Dion–Jacobson Two-Dimensional Perovskite Solar Cells. *Nano Lett.* **2019**, *19*, 150–157.
- (4) Mao, L.; Tsai, H.; Nie, W.; Ma, L.; Im, J.; Stoumpos, C. C.; Malliakas, C. D.; Hao, F.; Wasielewski, M. R.; Mohite, A. D.; Kanatzidis, M. G. Role of Organic Counterion in Lead- and Tin-Based Two-Dimensional Semiconducting Iodide Perovskites and Application in Planar Solar Cells. *Chem. Mater.* **2016**, *28*, 7781–7792.